

RESULTS OF THE FIRST TESTS OF THE SIDRA SATELLITE-BORNE INSTRUMENT BREADBOARD MODEL

O. V. Dudnik^{1}, E. V. Kurbatov¹, A. M. Avilov¹, M. Prieto², S. Sanchez²,
A. V. Spassky³, K. G. Titov¹, J. Sylwester⁴, S. Gburek⁴, P. Podgórski⁴*

¹*V.N. Karazin Kharkov National University, Svobody Square, 4, 61022 Kharkov, Ukraine,*

E-mail: Oleksiy.V.Dudnik@univer.kharkov.ua;

²*Space Research Group, Alcala University, Alcala de Henares, Spain, E-mail: mpm@aut.uah.es;*

³*Skobeltsyn Institute of Nuclear Physics, Lomonosov Moscow State University, Moscow, Russia,*

E-mail: aspass@yandex.ru;

⁴*Solar Physics Division, Space Research Center, Kopernika str., 11, 51-622, Wroclaw, Poland,*

E-mail: js@cbk.pan.wroc.pl, sg@cbk.pan.wroc.pl, pp@cbk.pan.wroc.pl

(Received February 26, 2013)

In this work, the results of the calibration of the solid-state detectors and electronic channels of the SIDRA satellite-borne energetic charged particle spectrometer-telescope breadboard model are presented. The block schemes and experimental equipment used to conduct the thermal vacuum and electromagnetic compatibility tests of the assemblies and modules of the compact satellite equipment are described. The results of the measured thermal conditions of operation of the signal analog and digital processing critical modules of the SIDRA instrument prototype are discussed. Finally, the levels of conducted interference generated by the instrument model in the primary vehicle-borne power circuits are presented.

PACS: 29.30.-h, 06.30.-k, 06.90.+v

1. INTRODUCTION

Scientific equipment, engineered for space research purposes, calls for thorough ground-based optimization and development of several models, each of them should undergo in specialized tests that emulate the different flight operation phases [1]. Scientific instruments accumulate data in the course of an experiment under harsh conditions like high vacuum, temperature variations in the range of operation, ionizing space radiation, as well as the close presence of other scientific and service equipment. The above factors have an effect on the equipment during its live. The need to take the above-listed outer space factors into account becomes still more urgent in those cases where the equipment is engineered to accomplish interplanetary missions, including those to study the Sun at a close distance [2-4]. In the latter case, thermal and radiation inputs received by the scientific instrument are higher than those received on scientific equipment on board space vehicles in near-Earth orbit. Therefore, different instrument models shall be comprehensive tested [5] under high-vacuum conditions and at different temperatures on the instrument-mounting platform. To reduce the tests costs, some adjustment and testing operations are performed with the use of a common model. In our case, the laboratory model of the

SIDRA (Space Instrument for Determination of Radiation environment) [6-10] compact satellite-borne energetic charged particle spectrometer-telescope was used for this purpose. The adjustments and tests performed in the laboratory model of SIDRA include the tuning of instrument electrical parameters, thermal and vacuum testing, calibration of detectors with the use of accelerated charged particles and radioactive isotopes and finally the electromagnetic compatibility tests.

This paper presents the test results of the breadboard model of the SIDRA compact instrument under conditions of high vacuum and with variation in temperatures from -34 to +50°C. It also shows the electromagnetic interference generated by the instrument model in the vehicle-borne primary power circuits, as well as the results of the detectors calibration with the use of electrons and heavy charged particles.

2. CALIBRATION MEASUREMENTS WITH ACCELERATED CHARGED PARTICLES

The performance of the detectors and the analog signal processing unit was tested with isotope radioactive sources and accelerated light nuclei in the cy-

*Corresponding author E-mail address: Oleksiy.V.Dudnik@univer.kharkov.ua

clotron located at the D.V. Skobel'syn Institute of Nuclear Physics of M.V. Lomonosov Moscow State University [11, 12]. The output signals of the sample and hold circuits, analyzed with the spectrometric 12-bit analog-to-digital converter (ADC) 4K CAIII-USB manufactured by the "Parsek"* Limited Liability Company, were used in the experiments.

The radioactive sources used in the tests were electrons (^{207}Bi) and-alpha particles (^{226}Ra). In the cyclotron tests, accelerated beams of protons, deuterons and α -particles with their energy levels being up to 7.5 MeV/nucleon were used. With the help of calibrated aluminum plates of different thickness at the detector inputs, similar particles with energy $E=7.5...21$ MeV were produced.

To extend the range of the linear part of recorded particle energies, the gain coefficient of the input test in the full absorption detector D2 was set to $C_g=3.8$. Only one energy line, with the highest energy at $E=1048$ keV, was used from among four energy lines of electrons of β -source ^{207}Bi , this signal that was recorded in the 32nd channel of the ADC. In the course of the experiment involving the use of α -particles the distance between source ^{226}Ra and detector was 4.02 mm; with such a distance the energy losses in air are $\Delta E=543$ keV. Hence, when plotting the appropriate graph, the source energy values $E_{\alpha 1}=4782$ keV, $E_{\alpha 2}=5490$ keV, $E_{\alpha 3}=6002$ keV, and $E_{\alpha 4}=7687$ keV were reduced by the value of losses in air.

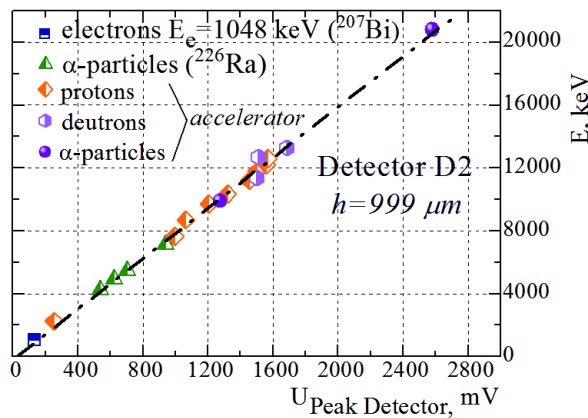


Fig. 1. Energy absorbed in D2 detector vs. analog signal processing channel amplitude at the peak detector output

From the obtained particle energy spectra, the values of the ADC channel numbers that correspond to the maximum values in the distributions of the number of particles with different energies were found. The ADC channel numbers were recalculated into amplitudes of output signals of peak detectors (PD) U_{PD} and the results obtained were summarized in one plot. Fig. 1 illustrates the dependence of full absorption energy in D2 detector vs. the amplitude of the analog signal U_{PD} at the output of the peak detector of the relevant electronic processing channel. It can be seen

that the experimental values obtained from different sources of accelerated charged particles can be linearly approximated with a good accuracy degree.

Thus, the proposed methods of combined calibration measurements, can be used to assess channel sensitivity at a chosen gain coefficient. This is done finding the maximum value of full absorption energy, following the measurement of the dynamic range of the peak detector operation with the help of a test signal. In addition, the obtained relationship represents one of the sources of the initial data intended for the development of the processing logics and software for the Field-Programmable Gate Array (FPGA) of the module for digital signals processing instrument prototype.

3. THERMAL AND VACUUM TESTING OF THE INSTRUMENT

To be able to simulate the temperature conditions and to enable the operation of the instrument and its separate modules in outer space, a special hot bench as part of the stationary vacuum plant was designed and manufactured. The hot bench consists of a copper plate that mounts a serpentine copper tube intended for cooling the bench with liquid nitrogen vapors, and a nichrome-wire heater made as a spiral, which is arranged within quartz sleeves. The copper tube and quartz sleeves are arranged within the copper plate grooves so that the maximum heat transfer rate can be provided. Such configuration also provides for regular heating across the whole upper service plane of the hot bench. The minimum temperature gradient across the surface and thickness of the bench is ensured thanks to a very good heating contact between the serpentine copper tube, heater and plate. In the lower part of the hot bench, and in order to provide thermal isolation with the vacuum chamber casing, four thermal 50 mm-high feet were used.

To maintain the hot bench temperature over the range of $\pm 1^{\circ}\text{C}$, a two-channel thermostat type TPM-202 is provided. It is able to ensure the operation in both heating and cooling modes. Heat is mainly transferred from the bench to the telescope parts to be tested due to their heat conductivity properties. The temperature of the instrument under test is controlled in different controlled points with the use of specially designed and calibrated chromel-alumel thermocouples.

The thermal and vacuum tests of the SIDRA instrument breadboard model were carried out with a pressure of $P=2...8 \times 10^{-5}$ Torr. This value depends on the rate of heating or cooling applied to the instrument. Vacuum condition was provided with the use of a high-pressure vacuum part and magnetic-discharge high-vacuum pump type HOPД-250.

The performance of the instrument model was tested under the following conditions: 1) constant temperature of the hot bench, maintained with the

*<http://www.parsek.ru>

use of a cooling agent; 2) heating the hot bench up to $+50^{\circ}\text{C}$; 3) slow cooling the hot bench down to -34°C .

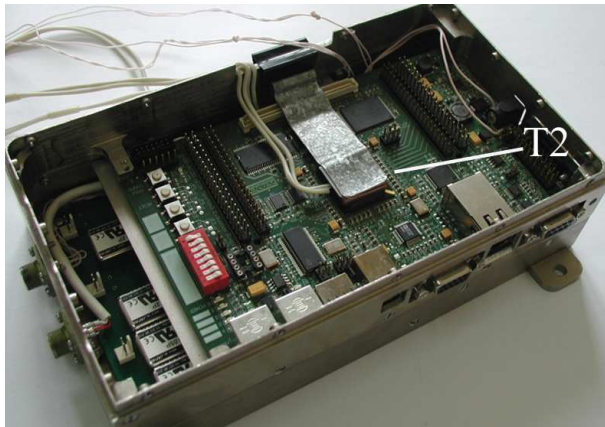


Fig. 2. Location of the thermocouple on the Xilinx Spartan 3 XC3S1500 FPGA in the GR-XC3S-1500 board

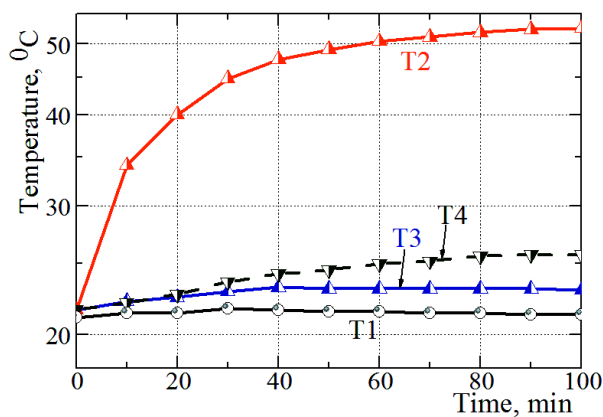


Fig. 3. Temperature distribution under high-vacuum conditions, at constant hot bench temperature

Prior to start the tests, special temperature-sensing elements were set in different points of the instrument—calibrated thermocouples made of chromel-alumel alloys: T1 – on the hot bench surface; T2 – on the surface of Xilinx Spartan 3 XC3S1500 FPGA; T3 – on the surface of radiator DC-DC of secondary power board converters; T4 – close to the signal analog processing module from the inner side of the instrument case. In Fig. 2, the setup of the tests and how the thermocouple is fixed to the surface of the Xilinx Spartan 3 XC3S1500 FPGA using a special galvanized-iron shaped bracket, is shown.

During the initial stage a water coolant with a controllable flow rate was used. The hot bench temperature was maintained constant and equal to $T \approx 21^{\circ}\text{C}$ during the 100-minute period of the experiment. Fig. 3 illustrates the distribution of the temperature values over the range of values indicated by 4 temperature-sensitive elements. 90...100 minutes

after the experiment began the FPGA surface temperature reached $\sim 53^{\circ}\text{C}$ and underwent no further practical changes. While the temperature on the FPGA surface made $\sim 40^{\circ}\text{C}$ under laboratory and atmospheric pressure conditions, the temperature increased by $\Delta T = 13^{\circ}\text{C}$ under vacuum conditions, at constant hot bench temperature and under condition of no convection and external heat radiators.

During the second stage of the experiment the hot bench was first heated up to $+40^{\circ}\text{C}$ and was held in this conditions for 140 minutes. From $t \approx 40$ minutes on, almost a complete thermal stabilization occurred (Fig. 4). The vacuum level reached $\sim 7 \times 10^{-5}$ Torr. Under those conditions the adhesive matter of the printed circuit boards and cable network started to outgassing. The temperature on the FPGA surface attained the level of $\sim 66^{\circ}\text{C}$. In Fig. 4 the horizontal dashed-dot line denotes at $T = 85^{\circ}\text{C}$ the upper temperature limit of the FPGA serviceability. Next, at 160...220 minutes since the experiment was started the hot bench temperature rose to the value of $+50^{\circ}\text{C}$.

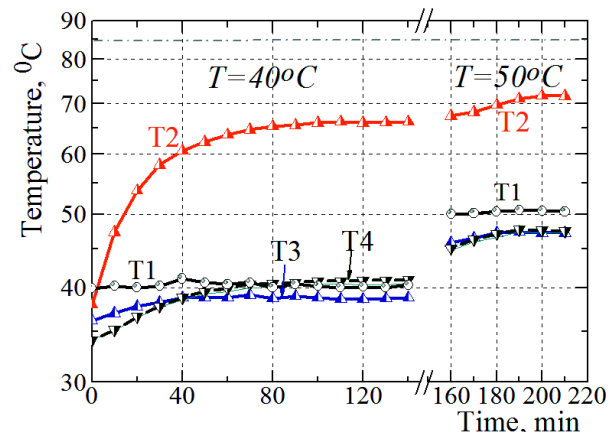


Fig. 4. Temperature distribution under high-vacuum conditions, with hot bench being heated up to $+40$ and $+50^{\circ}\text{C}$

The FPGA surface temperature attained the value of $+72^{\circ}\text{C}$, while the remaining parts and modules of the instrument almost reached the hot bench temperature. At this final stage the difference between the hot bench temperature, and FPGA surface was $\Delta T = 22^{\circ}\text{C}$.

Fig. 5 presents the temperature pattern distribution when the hot bench was cooled with the use of liquid nitrogen vapors during a period of 170 minutes. The cooling system was disconnected on minute 171, and the heat was transferred from the vacuum chamber outer walls to the inner walls till the end of the experiment (minute 200). The residual atmosphere pressure inside the chamber varied from 4.2×10^{-5} to 1.4×10^{-5} Torr under the lowest temperature conditions. Despite the continuous decrease in hot bench and boards temperature during the initial 60 minutes, the FPGA surface temperature kept growing to attain the value of $T = 42^{\circ}\text{C}$ in minutes 50...60. All the

instrument's modules attained the negative temperature of $T=-34^{\circ}\text{C}$, but the FPGA surface that was still positive, $T=12^{\circ}\text{C}$.

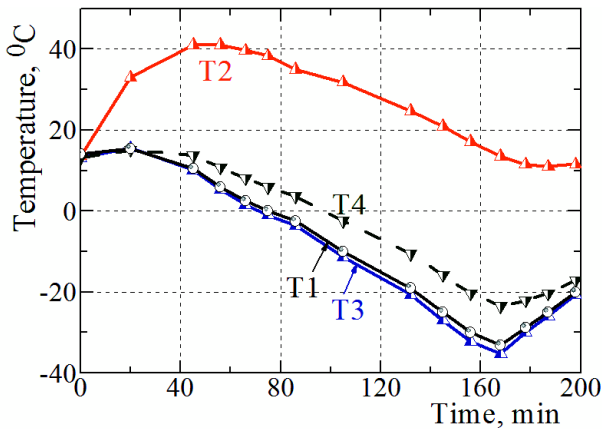


Fig.5. Temperature distribution under high-vacuum conditions, with hot bench being cooled down to -34°C

The breadboard model of the SIDRA instrument demonstrated its serviceability under high vacuum conditions with hot bench temperature going down to -34 and up to $+50^{\circ}\text{C}$. At the same time, the installation of the heat-eliminating radiator on the surface of DC-DC converters of the secondary power board was proved correct and there was found necessary that a similar radiator be installed on the FPGA surface.

4. MEASUREMENTS OF ELECTROMAGNETIC INTERFERENCE GENERATED BY INSTRUMENT BREADBOARD MODEL IN POWER CIRCUITS

When functioning as part of the satellite, scientific equipment should remain stable to the effects of the electromagnetic interference generated by some other scientific devices and satellite servicing systems and, simultaneously, should not cause any harmful influence on them. For this reasons it is necessary to conduct the electromagnetic compatibility (EMC) tests. The permissible interference levels should be set in the technical documents pertaining to the equipment. The tests should be conducted at the stage of the models development and manufacture to prove the correctness of schematic solutions.

One of the types of electromagnetic effects is the conducted interference in power circuits. The impact of this interference depends on different factors such as the choice of circuitry, the application of structural and circuit designs in the form of electric and magnetic screens, the use of electric filters, the protective grounding and the optimum electric circuit routing. To assess the engineering solution that we adopted, there were made prior measurements of the levels of inductive interference which are generated by the instrument model in the primary power circuit. To avoid the voltage and magnetic interferences

produced by the electric network ($U=220\text{ V}$ and frequency $f=50\text{ Hz}$), two storage batteries, having total potential difference of $U=25.5\text{ V}$ were used to supply power to the SIDRA instrument model. Fig. 6 shows the measurement unit circuit.

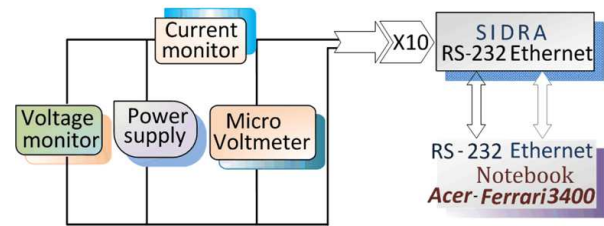


Fig.6. Block scheme of the experiment used to measure the levels of conducted interference generated by SIDRA instrument in primary power circuits

Noise levels were measured with the use of microvoltmeter B3-57 with a frequency range between 5 Hz to 9 MHz and a Polish-production selective microvoltmeter WMS-4, operating in the frequency range from 30 to 300 MHz.

In order to control the serviceability of the instrument model, imitate the passage of particles through the detector system, enable the reception of digital signals by the monitoring computer and observation of analog signals, different instrumentation was used. Among them a Tektronix TDS 2012 oscilloscope, a Tektronix AFG 310 arbitrary-shape signal generator and an Acer-Ferrari 3400 portable personal computer. With the microvoltmeter B3-57, the measurements were made in two ranges $\Delta f_1=5\text{ Hz...}50\text{ kHz}$, and $\Delta f_2=5\text{ Hz...}9\text{ MHz}$. In Fig. 7 the experimental equipment used to measure conducted interference levels is shown.

Table 1. Peak values of conducted interference in high-frequency range, generated by SIDRA instrument breadboard model in primary power circuits

Number of subrange	Borders of subrange, MHz	Value of interference, μV
1	30...35	20
2	35...50	14
3	50...99	20
4	100...109	36
5	110...300	17

According to the measured results, the values of effective conducted interference U_{ef} generated by the SIDRA instrument in primary power circuit $U=25.5\text{ V}$, were as follows: $U_{ef} \sim 700\ \mu\text{V}$ in the first frequency range and $U_{ef} \sim 121\ \mu\text{V}$ in each arbitrary subrange $\Delta f=50\text{ kHz}$ of general range Δf_2 . Table 1 presents the results of measurements of conducted interference peak values U_{peak} in the high-frequency range thanks to the use of selective microvoltmeter WMS-4. The peak level of the interference values

generated in the 4th frequency subrange is somewhat higher than in the neighboring subranges. However, all measured values are sufficiently low, as compared to the relevant standard requirements. The measure-

ments that were made over the range of frequencies from 5 Hz to 300 MHz demonstrated the correctness of choice of the elemental composition and arrangement of the instrument secondary power module.



Fig.7. Experimental equipment used to measure the conducted interference levels

CONCLUSIONS

In this work the results of the calibration of the SIDRA instrument breadboard model with charged particles accelerated in a cyclotron accelerator of medium-energy nucleons and derived from radioactive isotopes, have been described. The results prove the linearity of the telescopic system detectors response and also the linearity of the analog signal processing channels. These methods can be used to assess the sensitivity of analog signal processing channels at a chosen gain coefficient, as well as to find the maximum values of full absorption energies, based on the preliminary measurement of the dynamic range of operation of the sample and hold circuit with the help of test signals.

Thermal and vacuum testing of the instrument laboratory model demonstrated its serviceability under condition of heating the model-mounting platform up to +50°C, as well as its cooling down to -34°C. At the same time, we realized that a heat-eliminating radiator should be installed on the surface of the Xilinx Spartan III FPGA, operating under high-vacuum conditions. The electromagnetic compatibility tests demonstrated a moderate level of radio-frequency interference in the frequency range 5 Hz ÷ 300 MHz, which were generated by the SIDRA instrument breadboard model in the vehicle-borne primary power circuits, thus proving the correctness of choosing filter circuits for the electrical network of the instrument secondary power module.

The work was carried out with the support of the Science and Technology Center in Ukraine, Grant No. 3542, University, city of Alcalá, Grant No. CCG08-UAH/ESP-3991, and Ministry of Science and Innovations in Spain, Grant No. ESP2005-07290-C02-02.

References

1. V.N. Yurov, V.G. Tyshkevich. The scientific equipment complex of the satellite CORONAS-Photon. Space flight experience // *Results of space experiment CORONAS-PHOTON. Propositions to the continuation of the program Coronas: scientific tasks and apparatus*. Russia, Moscow, Space Research Institute, 2012, p. 7-18 (in Russian).
2. D. Muller, R.G. Marsden, O.C. St. Cyr, H.R. Gilbert. Solar Orbiter. Exploring the Sun-Heliosphere connection // *Solar Phys.* 2012, DOI: 10.1007/s11207-012-0085-7.
3. W.I. Axford, E. Marsch, V.N. Oraevsky, V.D. Kuznetsov, T.K. Breus, et al. Space mission for exploration of the Sun, Mercury and inner heliosphere ("InterHelios") // *Adv. Space Res.* 1998, v. 21, N1-2, p. 275-289.
4. V.D. Kuznetsov, V.N. Oraevsky. Polar-Ecliptic Patrol (PEP) for Solar Studies and Monitoring of Space Weather // *Journ. British Interplanetary Soc.* 2002, v. 55, N11-12, p. 398-403.

5. A.V. Dudnik, V.K. Persikov, I.I. Zalyubovsky, T.G. Timakova, E.V. Kurbatov, Yu.D. Kotov and V.N. Yurov. High sensitivity STEP-F spectrometr-telescope for high-energy particles of the CORONAS-PHOTON satellite Experiment // *Solar Syst. Res.* 2011, v.45, N3, p. 212–220.
6. O.V. Dudnik, D. Meziat, M. Prieto. The concept of compact on-board instrument for measurements of particle fluxes and dose rates // *Scientific Session of Moscow Engineering Physics Institute-2009*, Moscow, Russia, Abstracts. 2009, v. 2. p. 151 (in Russian).
7. O.V. Dudnik, V.V. Bilogub, E.V. Kurbatov, T.G. Timakova, V.N. Dubina, D. Meziat, M. Prieto. Compact on-board instrument SIDRA for measurement of particle fluxes and dose rates – concept and first model // *9th Ukrainian Conf. on space research*. Crimea, Ukraine. Abstracts, 2009, p. 78.
8. O.V. Dudnik, M. Prieto, E.V. Kurbatov, S. Sanchez, T.G. Timakova, V.N. Dubina, P. Parra. First concept of compact instrument SIDRA for measurements of particle fluxes in the space // *Journ. of Kharkov University, phys. series "Nuclei, Particles, Fields"*. 2011, v. 969, iss. 3(51), p. 62-66.
9. O.V. Dudnik, S. Sanchez, M. Prieto, E.V. Kurbatov, T.G. Timakova, V.N. Dubina, P. Parra. Onboard instrument SIDRA prototype for measurements of radiation environment in the space // *39th Scientific Assembly of the Committee on Space Research. July 14-22, 2012*. Mysore, India. Abstracts. Session H0.3: "Technical Development of Instrumentation for Current Missions", STW-B-153 H0.3-0023-12. p. 106.
10. O.V. Dudnik, M. Prieto, E.V. Kurbatov, S. Sanchez, T.G. Timakova, K.G. Titov, P. Parra. Small-sized device for monitoring of high energy electrons and nuclei in the open space // *Space Sci. and Tech.* 2012, v. 18, N6, p. 22-34 (in Russian).
11. L.A. Sarkisyan, E.F. Kiryanov, Yu.A. Vorobyov. Modernization of 120-cm's cyclotron // *Pribory i Tekhnika Eksperimenta*. 1979, v. 24, N1, p. 19-21 (in Russian).
12. E.F. Kirjanov, A.V. Spassky. 120-cm centimeter cyclotron of the Skobel'syn Institute of Nuclear Physics of the Lomonosov Moscow State University // *Researches on nuclear and atomic physics on cyclotrons of the SINP of the MSU*. Russia, Moscow, Moscow State University, 2009, p. 44-52 (in Russian).

РЕЗУЛЬТАТЫ ПЕРВЫХ ИСПЫТАНИЙ ЛАБОРАТОРНОГО МАКЕТА СПУТНИКОВОГО ПРИБОРА SIDRA

*А.В. Дудник, Е.В. Курбатов, А.М. Авиллов, М. Прето, С. Санчез, А.В. Спасский,
К.Г. Титов, Я. Сильвестер, Ш. Гбурек, П. Подгурски*

Представлены результаты градуировки твердотельных детекторов и электронных каналов лабораторного макета спутникового спектрометра-телескопа энергичных заряженных частиц SIDRA. Описываются блок-схемы и экспериментальное оборудование для проведения тепловакуумных испытаний узлов и модулей компактной спутниковой аппаратуры и для осуществления испытаний научных приборов на электромагнитную совместимость. Обсуждаются результаты измеренных тепловых режимов работы критических узлов модулей аналоговой и цифровой обработок сигналов прототипа прибора SIDRA. Наконец, представлены уровни кондуктивных помех, создаваемых макетом прибора в цепях первичного бортового питания.

РЕЗУЛЬТАТИ ПЕРШИХ ВИПРОБУВАНЬ ЛАБОРАТОРНОГО МАКЕТУ СУПУТНИКОВОГО ПРИБОРУ SIDRA

*О.В. Дудник, Е.В. Курбатов, А.М. Авиллов, М. Прето, С. Санчез, А.В. Спасский,
К.Г. Титов, Я. Сильвестер, Ш. Гбурек, П. Подгурски*

Представлено результати градування твердотільних детекторів і електронних каналів лабораторного макету супутникового спектрометру-телескопу енергійних заряджених частинок SIDRA. Описуються блок-схеми і експериментальне обладнання для здійснення тепловакуумних випробувань вузлів і модулів компактної супутникової апаратури та для проведення випробувань наукових приладів на електромагнітну сумісність. Обговорюються результати вимірювань теплових режимів роботи критичних вузлів модулів аналогової і цифрової обробки сигналів прототипу приладу SIDRA. Нарешті, представлені рівні кондуктивних завад, що створює макет приладу в ланцюгах первинного бортового живлення.